Title

Experimental investigation of large-scale flow structures in an aircraft cabin mock-up.

Authors

Zhang, Yongzhi

Li, Jiayu

Liu, Mingxin

et al.

Publication Date

2020-10-15

DOI

10.1016/j.buildenv.2020.107224

Peer reviewed

Since January 2020 Elsevier has created a COVID-19 resource centre with free information in English and Mandarin on the novel coronavirus COVID-19. The COVID-19 resource centre is hosted on Elsevier Connect, the company's public news and information website.

Building and Environment 184 (2020) 107224

Contents lists available at ScienceDirect

Building and Environment

journal homepage: http://www.elsevier.com/locate/buildenv

Experimental investigation of large-scale flow structures in an aircraft cabin mock-up

Yongzhi Zhang [a], Jiayu Li [b], Mingxin Liu [c], Junjie Liu [c,*], Congcong Wang [d]

[a] College of Environmental Science and Engineering, Donghua University, Shanghai, 201620, China
[b] Berkeley Education Alliance for Research in Singapore, 138602, Singapore
[c] Tianjin Key Laboratory of Indoor Air Environmental Quality Control, School of Environmental Science and Engineering, Tianjin University, Tianjin, 300072, China
[d] School of Environment and Energy Engineering, Beijing University of Civil Engineering and Architecture, Beijing, 100044, China

ARTICLE INFO

Keywords:
Aircraft cabin
Turbulence kinetic energy spectra
Large-scale circulation
Thermal plume
Airflow

ABSTRACT

The purpose of this study was to investigate the influence of large-scale circulation on the flow field in a cabin mockup. The velocity was measured by ultrasonic anemometers (UA). Then, this study analyzed the turbulence kinetic energy spectra of the velocity fluctuation signal. The turbulence kinetic energy spectra of the measurement points reflect the flow characteristic of the large-scale circulation in the cabin mockup. The results contribute to the understanding of the role of the thermal plume on the large-scale circulation in the cabin. The large-scale circulation's impact on air quality was also investigated, and the contaminant distribution was measured using tracer gas in the cabin. The two large-scale circulation interactions made the air flow mixing approximately uniform.

1. Introduction

The civil airliner is an important means of transport that has greatly reduced people's travel time. Increasing numbers of people use aircraft for travel. The aircraft brings convenience to passengers but has also increased air quality problems [1]. The cabin environment has a high density of occupants, increasing the risk of passenger cross-infection [2]. There is a mutual coupling effect between the supply-air jet and the human thermal plume, an effect which makes the flow field more complicated in the cabin. Therefore, investigating the flow characteristics within the cabin is necessary during commercial passenger flights [3]. A mixing ventilation system is commonly used in the aircraft cabin; the system consists of air supply at the top of the cabin and exhaust air at the bottom. Due to the mixing characteristic, the system can disperse infectious diseases through airflow in the cabin [4]. The mixing ventilation system is not conducive to the exclusion of contaminants. The characteristics of the mixture can more easily allow airborne transmission of infectious disease in the cabin [5]. The novel coronavirus (2019-nCoV) outbreak led many countries to the screening of travelers for respiratory symptoms and febrile illness [6,7]. Obviously, the civil airliner acts as a carrier of virus transmission.

The supply-air jet enters the cabin with a certain momentum, and the two supply-air jets collide in the aisle region. The thermal plumes are unstable and limited by the small space [9]. The supply-air jets have high turbulence intensity. The supply-air jet and the thermal plume from passengers mix with each other, forming large-scale circulation. The supply-air jets' collision of airflow takes place in the middle region of the cabin mockup. This means that the flow has a more complex structure in the middle region of the cabin [10]. The large-scale eddies dominate the overall flow structures at higher supply air velocities [8]. Passengers near the aisle are more susceptible to infection [11]. According to Körner et al.'s research, the oscillation of the two supply-air jets causes the velocity oscillations of the flow field [12]. The coherent oscillation of the large-scale circulation structure depends on the Reynolds number. The empirical model describes the two collision supply-air jets and the automatic oscillation with respect to the geometric relation of the inlet and Reynolds number. In addition, current studies have shown that simplified geometric models were well suited for indoor large-scale circulation ventilation problems [13]. The room geometry can be used to distinguish between unstable to stable room airflow structures [35]. Through Yan's experiment and computational fluid dynamics (CFD), it was found that the location of the pollution source had a significant effect on the transport of pollutants in the cabin [14]. It was also found that an increased ventilation rate does not necessarily protect the passengers close to the source. This is due to the characteristics of the large-scale circulation of the flow field.

* Corresponding author. Room 228, Building 14, Tianjin University, Tianjin 300072, China.
E-mail address: jjliu@tju.edu.cn (J. Liu).

https://doi.org/10.1016/j.buildenv.2020.107224
Received 28 April 2020; Received in revised form 3 August 2020; Accepted 20 August 2020
Available online 29 August 2020

To fully understand the complex airflow in the cabin, it is necessary to fully study the characteristics of large-scale circulation. Knowledge of the spatial and temporal characteristics of large-scale circulation is becoming increasingly important. The related research can guide the design of the cabin. The thermal plume and supply-air jet momentum-driven flow have highly complex structures. Bosbach et al. analyzed the interactions between supply-air jets and thermal plumes under two different air inlet configurations [15]. The large-scale airflows have random and unstable spatial and temporal flow structures. Large-scale convective transport depends on the dynamic structure of the flow. Heat transfer is determined by the interaction of forced convection (FC) and thermal convection (TC) under mixed convection (MC). In particular, the turbulent mixed convection has attracted the interest of research scholars during the last decades [16,17]. Understanding large-scale circulation (LSC) is important for understanding the mechanism of turbulent convective energy transfer [18,19].

The high thermal load due to high occupant density has an effect on the flow field that is comparable in importance to the supply air jet. These competing flows cause instability [20–22]. Due to the heat dissipation of the passengers, the thermal boundary condition of the cabin's thermal environment was similar to Poiseuille-Rayleigh-Benard (PRB) mixed convection flows [23]. From a technical point of view, the dynamics of the large-scale circulation and the effect of spatial distribution on thermal convection are very important [24]. In addition, the large-scale circulation was constantly fluctuating during the exercise [25]. The large-scale circulation was driven mainly by the supply-air jet in the cabin. The airflow dissipation downstream occurred at a lower frequency, which was due to the turbulence dissipation spectra [26,27]. The instantaneous velocity vector field obtained by the particle image velocity (PIV) can detect the core and center position of the large-scale circulation through a proper orthogonal decomposition algorithm. The three-dimensional nature of the large-scale circulation structure is represented by the irregular oscillating shape of the core line [28,29].

Spectral analysis is a commonly used method to study velocity fluctuation. The turbulence kinetic energy spectra index is an important parameter for characterizing the energy distribution on the double logarithmic power spectral density curve. The turbulence oscillation is not a completely random motion, but an irregular oscillation containing identifiable ordered large-scale motion. The development of the large-scale structures determines the distribution of oscillation in the flow field. The most important application of the existence of ordered structures in turbulence is that the turbulence can be controlled by interfering with such large-scale structures, resulting in a flow field with different spectra. The turbulence is superposed by different scales of vortices. The power spectral density function of the spectral analysis method can give the frequency and the fluctuation energy of the different vortices in the turbulence and can explain the flow field characteristics comprehensively and accurately.

With the maturity of the statistical theory of turbulence, and instruments capable of measuring high-frequencies, supply-air jet research began to focus on spectral characteristics. According to the statistical theory of turbulence, the spectrum carries all the information of turbulence. Saddoughi measured the velocity fluctuations through experiment, and verified the local-isotropy predictions of Kolmogorov's universal equilibrium theory. Kolmogorov time scale $\tau_K = (\gamma/\varepsilon)^{1/2}$ is used to normalize the frequency f, where, ε is the dissipation rate, γ is the Kinematic viscosity [30]. Fellouah et al. found that the frequency spectrum of the supply-air jet has a significant Re-number-dependent effect [31]. In the case of high Reynolds numbers, the velocity turbulence kinetic energy spectra of the supply-air jet have a significant inertial subrange. In the case of low Re numbers, the energy is directly transferred from the large-scale energetic zone to the small-scale dissipation region. The explanation of the three power law intervals are as follows: the interval of $-5/3$ represents the inertia subrange, the interval with a slope of -3 reflects the two-dimensional nature of turbulence, and the interval with a slope of -7 represents a small-scale dissipation region [32]. Mi et al. also did similar research. The variation of the spectral curve with the Re number of the supply-air jet was investigated [33]. It was found that the spectrum has a distinct inertial subregion only after the critical Reynolds number is exceeded.

The performance of large-scale flow structures was studied in an aircraft cabin mock-up. The purpose of this study was to evaluate the large-scale circulation impact on the cabin environment and the thermal plume impact on the flow field. This study used fast Fourier transform (FFT) algorithms to investigate the thermal plume's impact on the large-scale circulation. Experimental research was conducted to obtain the contaminant concentration, temperature field and flow field of the cabin mockup by using a trace gas and ultrasonic anemometer measurement system.

2. Methods

2.1. Experimental facility

The research set up a measurement device for obtaining the accurate temperature and velocity in a seven-row cabin mockup, as shown in Fig. 1. The dimensions of the cabin at floor level was 5.8 m (length) × 3.25 m (width), while the height of ceilings was up to 2.15 m from the floor. Forty-two thermal manikins were placed in the seats and simulated the effect of the passenger position on the airflow patterns. The heat load of each thermal manikin was set to 75 W. Air was supplied to the aircraft cabin mock-up by slot diffusers on each side, which were located under the overhead compartment. The supply air temperature from the diffusers was controlled at 19 ± 0.5 °C.

2.2. Measurement method

2.2.1. Velocity measurement

Under the cooling condition (CL), all the thermal manikins were turned on. Under the isothermal condition (ISO), all the thermal manikins were turned off. Ultrasonic anemometers (UA) were used to obtain velocity magnitude and direction, with a measurement range from 0 to 10 m/s and an accuracy of ±0.03 m/s. The measurement was performed at the middle cross-section of the manikins' legs in row 4, 15 cm in front of the fourth seat row of thermal manikins. The measurement lasted for 2 h. The sampling rate was constant at 20 Hz for each velocity component at a location. The velocity vector of the flow field is shown in Fig. 2. To investigate the thermal plume's impact on the large-scale circulation, the measurement point with almost zero 2-D velocity was taken as the center position of the large-scale circulation in the cabin. The measurement points were distributed along the large-scale circulation flow

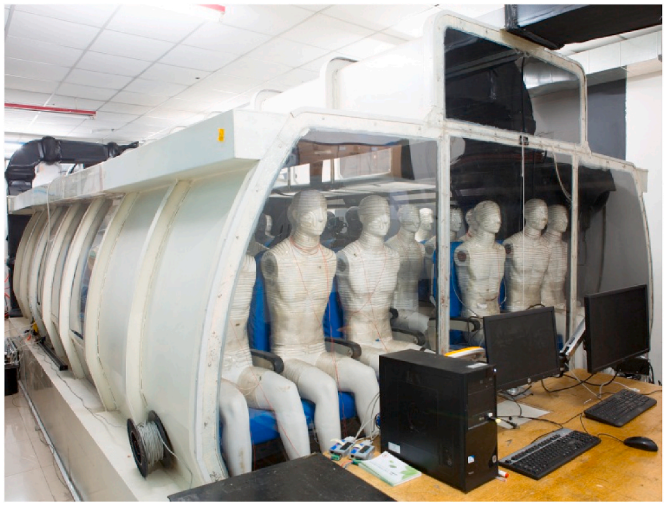

Fig. 1. The experimental facility cabin mockup.

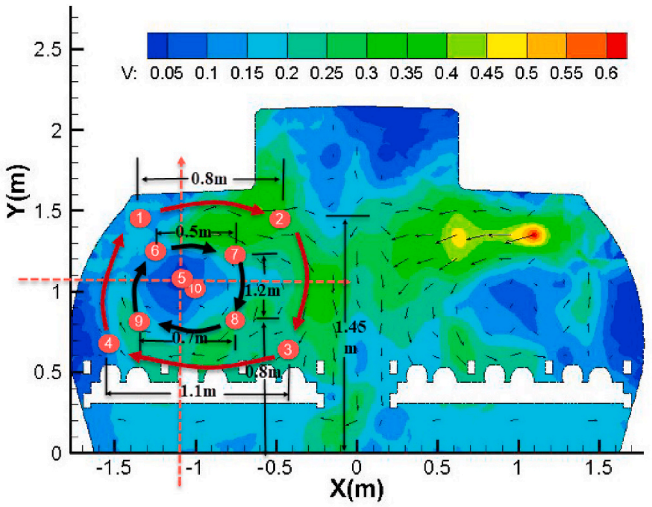

Fig. 2. Large-scale circulation measurement point distribution.

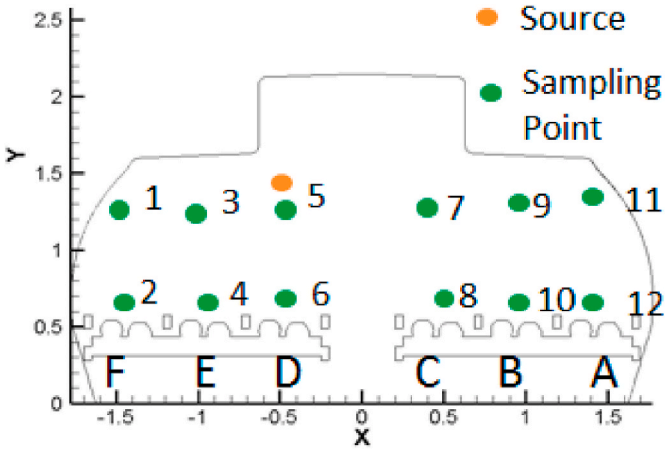

Fig. 3. Tracer gas sampling point distribution.

trajectories. The large-scale circulations have unsteady characteristics in the cabin, and the transient airflow patterns are also changeable [34]. In order to experimentally explore the representative position of turbulent kinetic energy spectrum analysis in the cabin, two case comparisons were performed in this study. The large-scale circulation's exterior trajectory was represented by a red line (case 1), while the large-scale circulation's interior trajectory was represented by a black line (case 2), as shown in Table 1 and Fig. 2. The measurement point distribution divides the space into 5 zones: supply-air jet zone (point 1 and point 6), collision zone (point 2 and point 7), recirculation zone (point 3 and point 8), entrainment zone (point 4 and point 9) and large-scale circulation center (point 5 and point 10). The different makes and models of airplanes use different designs and locations of air supply diffusers, so the results of this study only apply to the similar air supply configuration.

2.2.2. Tracer gas measurement

To investigate the large-scale circulation impact on the cabin environment, the contaminant distribution was measured using tracer gas in the cabin. Sulfur hexafluoride (SF_6) was used as the tracer gas due to safety and stability. The multigas monitor (Innova 1412, LumaSense Technologies, Ballerup, Denmark) and the multipoint sampler (Innova 1309) were selected as the gas measurement instruments. The accuracy of the tracer gas measurement system was 0.01 ppm, and the repeatability was 1% of the measured values. During the experiment, 1% SF_6 was released with a volume flow rate of 1 L/min at the location of the thermal manikin's mouth (in seat 4D). The sampling point locations were monitored by the INNOVA 1412, as shown in Fig. 3. The measurements took place in the same seat row as the source. Sample integration time was 5s, flushing times was 10s, and response times was 27s.

2.3. Analysis method

2.3.1. Fast fourier transform (FFT)

The velocity fluctuates with time series at the center position of the large-scale circulation, as shown in Fig. 4. In the time series, the velocity fluctuation is intense. It is necessary to convert the velocity fluctuation signal from the time series into the frequency series. The fast Fourier transform (FFT) is one of the most important algorithms in signal processing and data analysis. Therefore, this study investigated the characteristics of large-scale circulation by analyzing the turbulence kinetic energy spectra characteristics of each measurement point.

Table 1
The measurement points of the two cases.

	Measurement point	Remark
Case 1	→ ②→ ③→ ④ ⑤ (Redline)	The points ⑤ and ⑩ are repeated measurements at the same measurement point
Case 2	⑥→ ⑦→ ⑧→ ⑨ ⑩ (Blackline)	

3. Results and discussion

The turbulence kinetic energy spectra of the two cases have similar results, as shown in Fig. 5. In particular, the turbulence kinetic energy spectra of case 1 (points 2, 3, 4 and 5) and case 2 (points 7, 8, 9 and 10) are almost the same. Therefore, the results imply the turbulence kinetic energy spectra of the measurement points reflect the flow characteristic of the large-scale circulation in an aircraft cabin.

The supply-air jets have higher energy at the initial segments, and then the energy gradually decays during movement. At measurement point 1, the energy of the supply-air jet maintains circulation movement. The turbulence kinetic energy spectra are different between the point 1 and the point 6, as shown in Fig. 5. Due to the point 1 is located at the supply-air jet's initial segment of the large-scale circulation with a higher turbulence kinetic energy. The kinetic energy at point 1 is evenly distributed across frequency, until decreasing above 1 Hz. The turbulent kinetic energy decreases sooner with the increase of frequency at point 6, and the oscillation of the high-frequency region is dissipation region dominated by viscous dissipation. Along the trajectory of circulation, energy is gradually attenuated. The turbulent kinetic energy with little attenuation from measurement point 2 to measurement point 3. The turbulence kinetic energy spectra of large-scale circulation at point 3 and point 5 have almost the same characteristics. At the central location of the large-scale circulation (point 5 and point 10), the average velocity is smaller, as shown in Fig. 2. It still has high energy. This is due to the center position of the large-scale circulation constantly fluctuating during movement. The velocity magnitude and direction are also fluctuating. Therefore, the average velocity is smaller. Moreover, the circulation has low turbulence kinetic energy at the entrainment process (point 4). At that point, the turbulent vortex structure breaks into a small-scale vortex structure, the peak of the turbulent kinetic energy spectrum disappears. The airflow mixed with supply-air jet flow through circulation entrainment.

As shown in Fig. 6, the turbulence kinetic energy spectra of cooling condition and isothermal condition are nearly identical in trend and magnitude at point 1 and point 2. This behavior is due to the airflow energy mainly coming from the supply jets, with the thermal plume having a weak effect. The turbulence kinetic energy of the low frequency region (f(Hz)<1Hz) of point 2 is higher than point 1. The turbulence kinetic energy of the high frequency region (10Hz > f(Hz) >1Hz) of

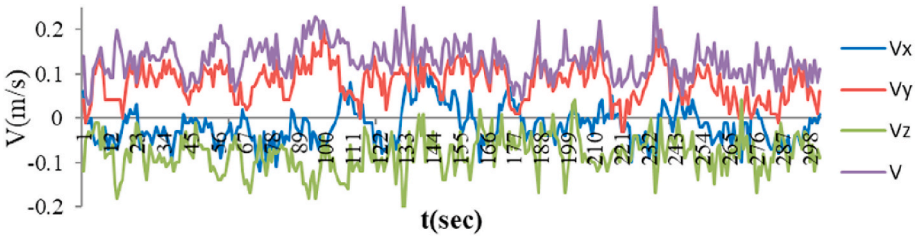

Fig. 4. Velocity fluctuations at point 5 in 300 s.

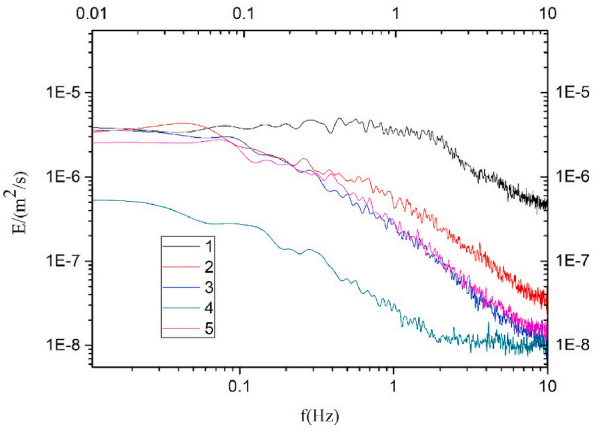

(1) Large-scale circulation's exterior turbulence kinetic energy spectra (Case 1)

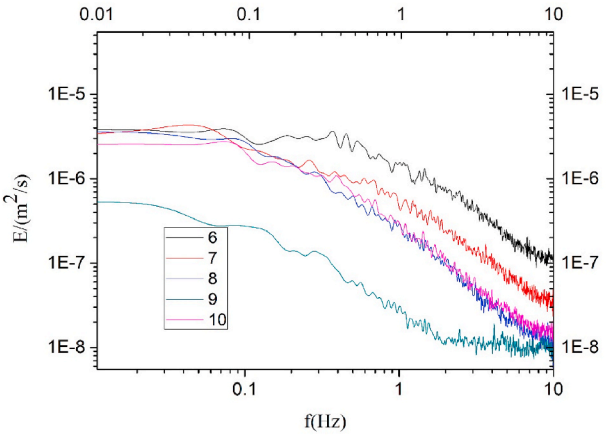

(2) Large-scale circulation's interior turbulence kinetic energy spectra (Case 2)

Fig. 5. The turbulence kinetic energy spectra of large-scale circulations under the cooling condition.
(1) Large-scale circulation's exterior turbulence kinetic energy spectra (Case 1)
(2) Large-scale circulation's interior turbulence kinetic energy spectra (Case 2).

point 1 is higher than point 2. It is due to supply-air jet attenuation; the energy slightly increases at the low frequency region.

For further investigation of the impact of human thermal plumes on airflow, ultrasonic anemometers (UAs) were used to obtain velocity magnitude. The turbulence kinetic energy spectra of the large-scale circulation were compared under the cooling condition (CL) and the isothermal condition (ISO). The red curves indicate cooling conditions, while the green curves indicate isothermal conditions. The horizontal axis is frequency, and the vertical axis is power.

As shown in Fig. 7 (1), under the isothermal condition, the turbulence kinetic energy of the high frequency region is decreasing. This is

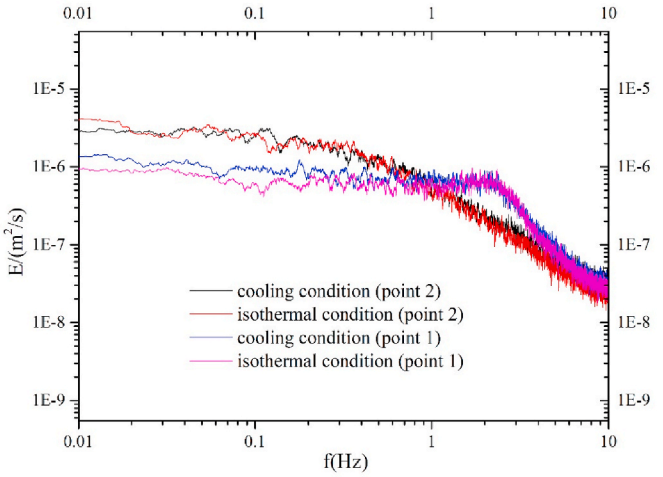

Fig. 6. The turbulence kinetic energy spectra under cooling condition (CL) and isothermal condition (ISO).

due to the weakening of the role of the supply-air jet at this region. The turbulence kinetic energy of the high frequency region (f(Hz) >1Hz) under the cooling condition is larger than the isothermal condition. Owing to the influence of the thermal plume, the airflows have more energy under cooling conditions at the high frequency region. Under the cooling condition, the thermal plume and the supply-air jet are mixed with each other and the turbulent dissipation of the supply-air jet is accelerated. Due to the influence of the thermal plume, the vortex structure is accelerated to dissipated. The turbulence kinetic energy dissipated from the large-scale circulation is increased at the high-frequency region. Therefore, the thermal plumes enhanced turbulent fluctuation at this region in the cabin.

At point 4, the turbulence kinetic energy of the low frequency region (f(Hz)<1Hz) under the cooling condition is larger than under the isothermal condition, as shown in Fig. 7 (2). This is due to the energy of the large-scale circulation is severely attenuated at this region. The occupant's thermal plume frequency is less than 1Hz. The thermal plume is mixed with the circulation and the energy of the low frequency region is enhanced. Under the cooling condition, due to the role of the circulation entrainment, the thermal plume and the circulation mixed with each other, increasing the energy of the large-scale circulation. At points 3 and 4, due to the influence of the thermal plumes, the large-scale circulation has more energy under cooling conditions at the process of circulation entrainment. The thermal plume can increase the energy of the larger-scale circulation at the lower frequencies.

At the large-scale circulation center (point 5), the turbulence kinetic energy spectra showed the same trend under both the cooling condition and the isothermal condition, as shown in Fig. 7 (2). This is because the passenger's thermal plume effect is small.

The turbulence kinetic energy spectra of the different regions are superposed as shown in Fig. 8. At the initial segment of the supply-air jet (points 1 and 2), the thermal plume of the passengers increased the

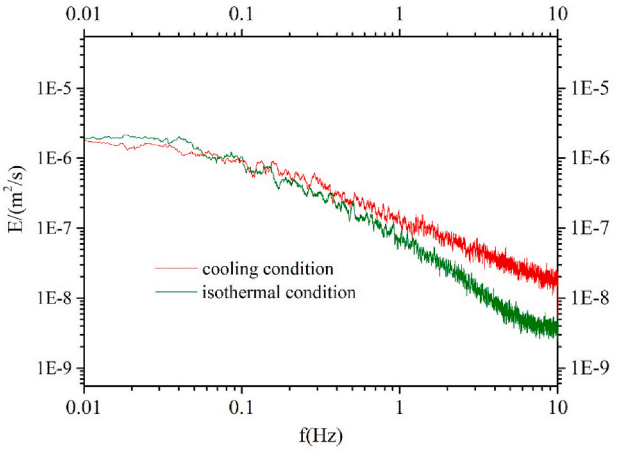

(1) Turbulence kinetic energy spectra at point 3

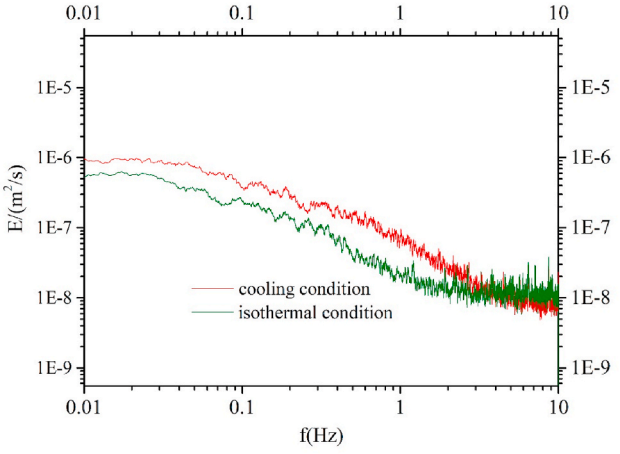

(2) Turbulence kinetic energy spectra at point 4

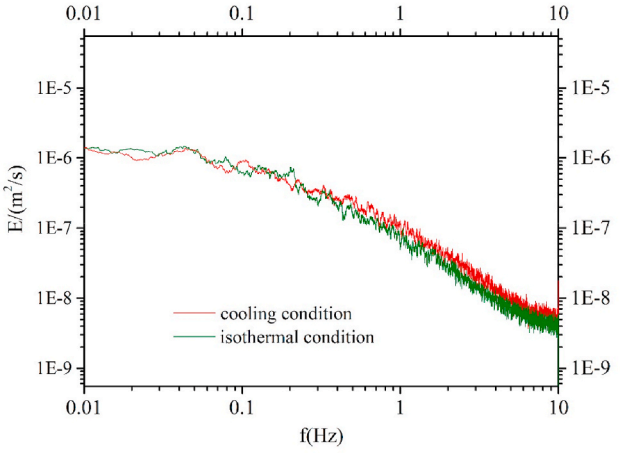

(3) Turbulence kinetic energy spectra at point 5

Fig. 7. The turbulence kinetic energy spectra under the cooling condition (CL) and the isothermal condition (ISO).
(1) Turbulence kinetic energy spectra at point 3
(2) Turbulence kinetic energy spectra at point 4
(3) Turbulence kinetic energy spectra at point 5.

circulation energy approximately by 10%. At the core of the rotation (point 5), the thermal plume increased the circulation energy approximately by 20%. At the bottom of the circulation (points 3 and 4), the thermal plume increased the turbulent energy approximately by 65%–75%. The thermal plume increased the energy of the large-scale circulation. Due to the influence of the thermal plume, the large vortices accelerated the transfer to the small vortex of the large-scale circulation. The results showed that the thermal plume had a significant effect on the circulation of the entrainment region. Therefore, the thermal plume contributed energy to the large-scale circulation, which enhanced the airflow mixing effect of the mixed ventilation system. The thermal plume is driven by the buoyancy force, which enhances the entrainment characteristics of the large-scale circulation. This helps to increase the uniformity of air mixing and helps the passengers dissipate heat in the cabin.

To investigate the role of the large-scale circulation in air distribution, the thermal manikin nearest the aisle was used as a source. The sampling point is shown in Fig. 3. The flow rate of tracer gas (1% SF_6) was constant at 1 L/min at the thermal manikin's mouth (point 5). The more detailed coordinate information and results are shown in Table 2. The source location was 5 cm above the point 5. The results show that the pollutants concentration is rapidly diluted by the large-scale circulation. The blue bar represents the concentration of pollutants at the passenger breathing zone, as shown in Fig. 9. The gray bar represents the concentration of pollutants at the circulation bottom region. The red bar is the contaminated source. Although the source was located on the left side of the cabin, the contaminants were also detected on the other side of the cabin. It is due to the interaction of two large scale circulations on both sides of the aisle in the cabin. Thus, the passengers are more likely to affect each other in the cabin on both sides of the aisle. The concentrations were not much different around the passengers on both sides of the aisle. This means that the two large-scale circulation interactions made the air flow mixing approximately uniform. Under the action of large-scale circulation, there is no phenomenon that the pollutants are completely locked. The effect of circulation is to rapidly dilute the pollutants through air mixing. The effect of circulation can make the velocity magnitude more uniform. Therefore, the mixing flow can control the level of pollutants.

4. Conclusions

To investigate the effect of large-scale circulation on the flow field in the cabin, the turbulence kinetic energy spectra of velocity fluctuation was obtained by fast Fourier transform (FFT). Then, the energy transfer mechanism of the large-scale circulation was analyzed. Under the mixing ventilation system, two large scale circulations inevitably formed in the cabin. Therefore, the passengers on both sides of the aisle had an increased likelihood of affecting each other in the cabin.

Firstly, the turbulence kinetic energy spectrum analysis method can well reveal the effect of thermal plumes on large-scale circulation in the cabin.

Secondly, the thermal plume transmitted energy to the large-scale circulation through the process of circulation entrainment at the bottom of the circulation.

Finally, the two large-scale circulation interactions made the air flow mixing approximately uniform. Under the mixing ventilation system, the large-scale circulation is the key factor affecting the airflow performance.

Declaration of competing interest

The authors declare that they have no known competing financial interests or personal relationships that could have appeared to influence the work reported in this paper.

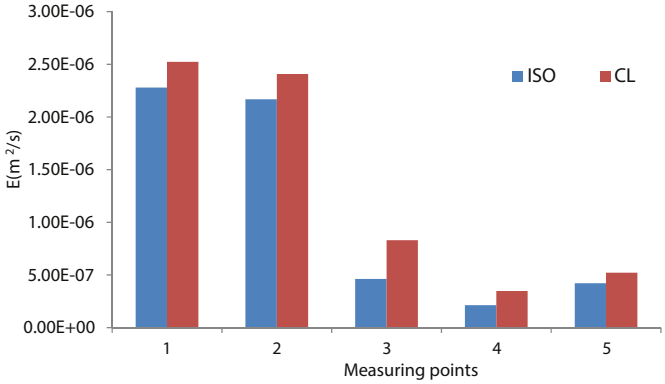

Fig. 8. The energy superposition of the large-scale circulation.

Table 2
The results of concentration and the local coordinates of the measurement locations.

Sampling point	1	2	3	4	5	Source	6	7	8	9	10	11	12
X (m)	−1.4	−1.4	−0.94	−0.94	−0.46	−0.46	−0.46	0.46	0.46	0.94	0.94	1.4	1.4
Y (m)	1.2	0.7	1.2	0.7	1.2	1.25	0.7	1.2	0.7	1.2	0.7	1.2	0.7
Concentration (ppm)	1.25	1.22	1.86	1.78	79.41	10000	2.84	0.66	1.06	0.72	0.95	0.99	0.86

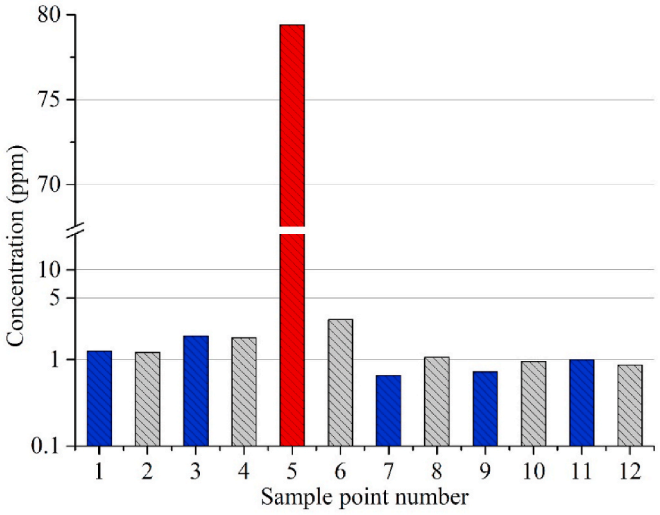

Fig. 9. Contaminant concentration distribution around passengers.

Acknowledgments

This study was supported by the National Natural Science Foundation of China (NSFC) through grant No. 51978452, the Tianjin Key Fundamental Research Program through grant No.14JCZDJC39200 and the National Basic Research Program of China (The 973 Program) through grant No. 2012CB720100.

References

[1] S.C. Lee, C.S. Poon, X.D. Li, F. Luk, Indoor air quality investigation on commercial aircraft, Indoor Air 9 (3) (1999) 180–187, https://doi.org/10.1111/j.1600-0668.1999.t01-1-00004.x.

[2] J.K. Gupta, C.H. Lin, Q. Chen, Transport of expiratory droplets in an aircraft cabin, Indoor Air 21 (1) (2011) 3–11, https://doi.org/10.1111/j.1600-0668.2010.00676.x.

[3] M. Wan, G. Sze To, C. Chao, L. Fang, A. Melikov, Modeling the fate of expiratory aerosols and the associated infection risk in an aircraft cabin environment, Aerosol. Sci. Technol. 43 (4) (2009) 322–343, https://doi.org/10.1080/02786820802641461.

[4] J. Fišer, M. Jícha, Impact of air distribution system on quality of ventilation in small aircraft cabin, Build. Environ. 69 (2013) 171–182, https://doi.org/10.1016/j.buildenv.2013.08.007.

[5] K. Gładyszewska-Fiedoruk, Indoor air quality in the cabin of an airliner, J. Air Transport. Manag. 20 (2012) 28–30, https://doi.org/10.1016/j.jairtraman.2011.10.009.

[6] M.E. Wilson, What goes on board aircraft? Passengers include Aedes, Anopheles, 2019-nCoV, dengue, Salmonella, Zika, et al, Trav. Med. Infect. Dis. 33 (2020), 101572, https://doi.org/10.1016/j.tmaid.2020.101572.

[7] B.J. Quilty, S. Clifford, S. Flasche, R.M. Eggo, Effectiveness of airport screening at detecting travellers infected with novel coronavirus (2019-nCoV), Euro Surveill. 25 (5) (2020), 2000080, https://doi.org/10.2807/1560-7917.ES.2020.25.5.2000080.

[8] C. Kandzia, D. Mueller, Flow structures and Reynolds number effects in a simplified ventilated room experiment, Int. J. Vent. 15 (1) (2016) 31–44, https://doi.org/10.1080/14733315.2016.1173291.

[9] J. Li, J. Liu, J. Pei, K. Mohanarangam, W. Yang, Experimental study of human thermal plumes in a small space via large-scale TR PIV system, Int. J. Heat Mass Tran. 127 (2018) 970–980, https://doi.org/10.1016/j.ijheatmasstransfer.2018.07.138.

[10] A.M. Padilla, Experimental Analysis of Particulate Movement in a Large Eddy Simulation Chamber, Kansas State University, 2008.

[11] H. Lei, Y. Li, S. Xiao, C.H. Lin, S.L. Norris, D. Wei, Z. Hu, S. Ji, Routes of transmission of influenza A H1N1, SARS CoV, and norovirus in air cabin: comparative analyses, Indoor Air 28 (3) (2018) 394–403, https://doi.org/10.1111/ina.12445.

[12] M. Körner, O. Shishkina, C. Wagner, A. Thess, Properties of large-scale flow structures in an isothermal ventilated room, Build. Environ. 59 (2013) 563–574, https://doi.org/10.1016/j.buildenv.2012.10.011.

[13] J. Bailon-Cuba, O. Shishkina, C. Wagner, J. Schumacher, Low-dimensional model of turbulent mixed convection in a complex domain, Phys. Fluids 24 (10) (2012), 107101, https://doi.org/10.1063/1.4757228.

[14] W. Yan, Y. Zhang, Y. Sun, D. Li, Experimental and CFD study of unsteady airborne pollutant transport within an aircraft cabin mock-up, Build. Environ. 44 (1) (2009) 34–43, https://doi.org/10.1016/j.buildenv.2008.01.010.

[15] J. Bosbach, M. Kühn, M. Rütten, C. Wagner, Mixed Convection in a Full Scale Aircraft Cabin Mock-Up vol. 715, 2006, pp. 3–8. ICAS2006, paper.

[16] D. Schmeling, A. Westhoff, M. Kühn, J. Bosbach, C. Wagner, Large-scale flow structures and heat transport of turbulent forced and mixed convection in a closed rectangular cavity, Int. J. Heat Fluid Flow 32 (5) (2011) 889–900, https://doi.org/10.1016/j.ijheatfluidflow.2011.06.006.

[17] D. Schmeling, J. Bosbach, C. Wagner, Oscillations of the large-scale circulation in turbulent mixed convection in a closed rectangular cavity, Exp. Fluid 54 (5) (2013) 1517, https://doi.org/10.1007/s00348-013-1517-3.

[18] M. Kaczorowski, O. Shishkina, A. Shishkin, C. Wagner, K.-Q. Xia, Analysis of the large-scale circulation and the boundary layers in turbulent Rayleigh-Bénard convection. Direct and Large-Eddy Simulation VIII, Springer, 2011, pp. 383–388, https://doi.org/10.1007/978-94-007-2482-2 61.

[19] O. Shishkina, C. Wagner, Modelling the influence of wall roughness on heat transfer in thermal convection, J. Fluid Mech. 686 (2011) 568–582, https://doi.org/10.1017/jfm.2011.348.

[20] W. Liu, R. Duan, C. Chen, C.-H. Lin, Q. Chen, Inverse design of the thermal environment in an airliner cabin by use of the CFD-based adjoint method, Energy Build. 104 (2015) 147–155, https://doi.org/10.1016/j.enbuild.2015.07.011.

[21] Y. Zhang, J. Liu, J. Pei, J. Li, C. Wang, Performance evaluation of different air distribution systems in an aircraft cabin mockup, Aero. Sci. Technol. 70 (2017) 359–366, https://doi.org/10.1016/j.ast.2017.08.009.
[22] C. Wang, J. Zhang, H. Chen, J. Liu, Experimental study of thermo-fluid boundary conditions, airflow and temperature distributions in a single aisle aircraft cabin mockup, Indoor Built Environ (2020), https://doi.org/10.1177/1420326X20932271.
[23] X. Nicolas, N. Zoueidi, S. Xin, Influence of a white noise at channel inlet on the parallel and wavy convective instabilities of Poiseuille-Rayleigh-Bénard flows, Phys. Fluids 24 (8) (2012), 084101, https://doi.org/10.1063/1.4737652.
[24] A. Westhoff, J. Bosbach, D. Schmeling, C. Wagner, Experimental study of low-frequency oscillations and large-scale circulations in turbulent mixed convection, Int. J. Heat Fluid Flow 31 (5) (2010) 794–804, https://doi.org/10.1016/j.ijheatfluidflow.2010.04.013.
[25] A. Westhoff, D. Schmeling, J. Bosbach, C. Wagner, Oscillations of large-scale structures in turbulent mixed convection in a rectangular enclosure. Advances in Turbulence XII, Springer, 2009, pp. 533–536, https://doi.org/10.1007/978-3-642-03085-7_128.
[26] S. Yao, Y. Guo, N. Jiang, J. Liu, Experimental investigation of the flow behavior of an isothermal impinging jet in a closed cabin, Build. Environ. 84 (2015) 238–250, https://doi.org/10.1016/j.buildenv.2014.10.024.
[27] Y. Guo, N. Jiang, S. Yao, S. Dai, J. Liu, Turbulence measurements of a personal airflow outlet jet in aircraft cabin, Build. Environ. 82 (2014) 608–617, https://doi.org/10.1016/j.buildenv.2014.10.007.
[28] M. Kühn, K. Ehrenfried, J. Bosbach, C. Wagner, Large-scale tomographic particle image velocimetry using helium-filled soap bubbles, Exp. Fluid 50 (4) (2011) 929–948, https://doi.org/10.1007/s00348-010-0947-4.
[29] D. Schmeling, J. Bosbach, C. Wagner, Measurements of the dynamics of thermal plumes in turbulent mixed convection based on combined PIT and PIV, Exp. Fluid 56 (6) (2015) 134, https://doi.org/10.1007/s00348-015-1981-z.
[30] S.G. Saddoughi, S.V. Veeravalli, Local isotropy in turbulent boundary layers at high Reynolds number, J. Fluid Mech. 268 (1994) 333–372.
[31] H. Fellouah, C. Ball, A. Pollard, Reynolds number effects within the development region of a turbulent round free jet, Int. J. Heat Mass Tran. 52 (17–18) (2009) 3943–3954, https://doi.org/10.1016/j.ijheatmasstransfer.2009.03.029.
[32] H. Fellouah, A. Pollard, The velocity spectra and turbulence length scale distributions in the near to intermediate regions of a round free turbulent jet, Phys. Fluids 21 (11) (2009), 115101, https://doi.org/10.1063/1.3258837.
[33] J. Mi, M. Xu, T. Zhou, Reynolds number influence on statistical behaviors of turbulence in a circular free jet, Phys. Fluids 25 (7) (2013), 075101, https://doi.org/10.1063/1.4811403.
[34] J. Li, J. Liu, X. Cao, N. Jiang, Experimental study of transient air distribution of a jet collision region in an aircraft cabin mock-up, Energy Build. 127 (2016) 786–793, https://doi.org/10.1016/j.enbuild.2016.06.039.
[35] C. Kandzia, D. Mueller, Stability of large room airflow structures in a ventilated room, Int. J. Vent. 17 (1) (2018) 1–16, https://doi.org/10.1080/14733315.2017.1332730.